http://dx.doi.org/10.5012/bkcs.2012.33.6.1972

Growth and Electrochemical Behavior of Poly[Ni(saldMp)] on Carbon Nanotubes as Potential Supercapacitor Materials

Yakun Zhang, Jianling Li,* Feiyu Kang,† Xindong Wang, Feng Ye,‡ and Jun Yang‡

*State Key Laboratory of Advanced Metallurgy, University of Science and Technology Beijing, No.30 College Road, Beijing 100083, China. *E-mail: lijianling@ustb.edu.cn*
†Department of Materials Science and Engineering, Tsinghua University, Beijing 100084, China
‡State Key Laboratory of Multiphase Complex Systems, Institute of Process Engineering, Chinese Academy of Sciences, Beijing 100190, China
Received February 3, 2012, Accepted March 18, 2012

The polymer of (2,2-dimethyl-1,3-propanediaminebis(salicylideneaminato))-nickel(II), Ni(saldMp), was deposited on multi-walled carbon nanotubes (MWCNTs) substrate by the route of potential linear sweep. The nano structures of poly[Ni(saldMp)] have been obtained by adjusting the monomer concentration of 0.1, 0.2, 0.5, 1.0 and 1.5 mmol L^{-1}. The poly[Ni(saldMp)] prepared in acetonitrile solution with monomer concentration of 1.0 mmol L^{-1} shows the fastest growth rate. The effects of potential window on charge-discharge efficiency and electrodeposition scan number on capacitance performance were discussed. Poly[Ni(saldMp)] prepared with less electrodeposition scans exhibits higher capacitance, but this goes against the improvement of the whole electrode capacitance. Sample with 8 deposition scans is the best compromise with the geometric specific capacitance 3.53 times as high as that of pure MWCNTs, and 1.24 times for the gravimetric specific capacitance under the test potential window 0.0-1.0 V.

Key Words : Redox polymer, Poly[Ni(saldMp)], Electrochemical polymerization, Supercapacitor

Introduction

Although transition metal oxides[1-6] and conducting polymers[7-11] have been widely studied as supercapacitor materials, only carbon-based materials including activated carbon,[12] carbon nanotubes[13-15] and graphene[16,17] have displayed promising electroperformance and stability. However, the use of these individual carbon materials in high-performance supercapacitors is limited due to their drawbacks, such as the unsatisfactory performance, the preparation complexity and the high cost. Therefore, incorporating some conducting polymers on the top of porous carbon materials[18,19] is one practical approach to get the aim of increasing electrochemical capacitance as well as lowering fabrication cost.

Conducting polymers such as polyaniline,[20-23] polypyrrole[14,24-26] and polythiophene[27,28] have been investigated as active materials for supercapacitors, which have advantage of high capacitance but drawback of stability. Transition metal complex with tetradentate N_2O_2 Schiff base ligand from salicylaldehyde and derivatives have been widely investigated in numerous scientific areas such as electrocatalysts, chemical sensors and magnetism. Oxidation of these metal complexes can lead to polymerization on conducting electrode surfaces in moderate/weak donor solvents and generate electroactive lms.[29] Anodic polymerization products of transition metal complex with tetradentate N_2O_2 Schiff base ligand possess reversible redox behavior, and it could be used for charge storage as supercapacitor materials.[30]

Electropolymerization is a particularly attractive method for preparing modified electrodes and is widely used for preparation of conducting polymer, metal and metal oxide. Linear sweep potential method, one of the most common electropolymerization method, was used for the electrodeposition of (Ni(saldMp)), which derivatives from the archetype of Schiff base metal complexes. Preparation parameters such as monomer concentration and number of electrodeposition scans were evaluated by cyclic voltammetry (CV) and galvanostatic charge/discharge (GC) tests. The reasonable electrochemical test window was confirmed, and the capacitance performance was estimated.

Experimental

Material Synthesis and Characterization. 2,2-Dimethyl-1,3-propanediamine (dMp, > 97%, GC,T) was supplied by J&K Chemica Co., Ltd. Acetonitrile (AN, > 99.9%, A.R. grade) was purchased from Guangdong Xilong Chemical Co., Ltd, while tetrabutylammonium perchlorate (TBAP, > 99.9%, C.P. grade) and triethylmethylammonium tetrauoroborate (Et_3MeNBF_4, > 99.9%, C.P. grade), ZhongSheng-HuaTeng Co., Ltd. The synthesized complex Ni(saldMp) monomer was recrystallized from AN, and its structure has been described in a previous paper.[31]

The specific surface area of multi-walled carbon nanotubes (MWCNTs) increased from 85 $m^2\ g^{-1}$ to 195 $m^2\ g^{-1}$ under reflux with concentrated HNO_3 and H_2SO_4 (volume ratio = 1/3) treatment. The MWCNTs electrode was prepared by the homodispersion of the carbon nanotube power in *N*-methyl-2-pyrrolidone (NMP) through sonication. The

slurry was coated on a Ti sheet (supported by BaoJiShi TuoPeng Metal Materials CO., Ltd. as current collectors) with the coating mass of 0.5 mg. The surface morphologies of poly[Ni(saldMp)] coated electrodes were measured by FESEM, using a Zeiss SuprATM[55] microscope.

Electrochemical Characterization. The electrodeposition of Ni(saldMp) and electrochemical measurements were carried out on a VMP2 electrochemical workstation with EC-Lab software (version 10.02) made by Princeton. The electropolymerization was conducted in a closed three-electrode compartment cell. The electrodeposition of Ni-(saldMp) on the resulting electrode (1 cm × 1 cm) was performed in AN solution which containing Ni(saldMp) complex monomer and 0.1 mol L^{-1} TBAP by linear sweep potential method between 0.0 and 1.2 V using an activated carbon sheet (1.5 cm × 2.5 cm) and a capillary Ag/AgCl wire as the auxiliary and reference electrodes, respectively, and the scan rate was 20 mV s^{-1}. The Ni(saldMp) complex monomer concentration for electrodeposition varied from 0.1 mmol L^{-1} to 1.5 mmol L^{-1}. The poly[Ni(saldMp)] electrodes were then washed in AN in order to remove any soluble species from the lm and were tested in a monomer-free solution of 1 mol L^{-1} Et_3MeNBF_4 in AN. CV and GC tests were measured with the same counter and reference electrodes and the electrochemical potential window was enlarged from 0.0-0.9 V to 0.0-1.2 V. All potentials in this article are given *vs.* Ag|AgCl.[32]

Results and Discussion

Effect of Concentration on Poly[Ni(saldMp)] Growth. It could come to the conclusion that the starting electropolymerization potential of Ni(saldMp) on MWCNTs is at least 0.4 V, which derives from the rst scan through the comparison of the MWCNTs and the composite electrodes in Figure 1. From the well-fined anode and cathode peaks, it can be easily confirmed the occurrence of the Ni(saldMp) polymerization on MWCNTs. It is clearly demonstrated that the deposition currents increase with the Ni(saldMp) concentration increasing from 0.1 mmol L^{-1} to 1.5 mmol L^{-1}, which means that more monomers are involved in the polymerization reaction. Attention should be paid to the appearance of a second oxidation peak, and it grows more and more obviously with the increase of the monomer concentration. This occurs as a result of the irreversible structure reorganization process of as-grown polymer (cross-linkage between pendant saldMp moieties)[33] arising from the growing concentrations.

The apparent surface coverage is another growth parameter to give an estimate for the actual surface coverage, which is calculated from the cyclic voltammetric anodic oxidation surface wave of the Ni(saldMp) polymerization and is adequate for monitoring the rate of polymer film growth at the electrode surface. Figure 2 shows the dependence of the apparent surface coverage on the scan number during the polymerization with the Ni(saldMp) concentrations varying from 0.1 mmol L^{-1} to 1.5 mmol L^{-1}. It is clear that the apparent surface coverage increases linearly with the number of polymerization scans under every concentration of Ni(saldMp), which indicates that more Ni(saldMp) monomers deposit on MNCNT to form polymer. From all the curves of various concentrations, the apparent surface coverage increases in different degree with the increasing deposition scan number under different concentrations. That is, the poly[Ni(saldMp)] growth rate is positively associated with the Ni(saldMp) concentration.

Figure 3 clearly describes the relationship between the polymerization rate and the Ni(saldMp) concentration. The polymerization rate is obtained from the slope of the line dependence of the apparent surface coverage on the electrodeposition scan number. Through beeline fitting, a linear increase of the polymerization rate with the Ni(saldMp) concentration under 1 mmol L^{-1} is observed, which means that the poly[Ni(saldMp)] growth rate increases in line with concentration when the concentration is below 1 mmol L^{-1}.

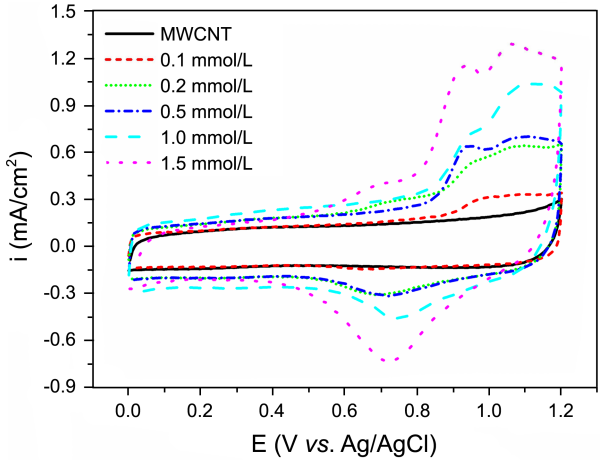

Figure 1. First scan of CV plots for anodic polymerization of Ni(saldMp) on MWCNTs with different monomer concentrations in 0.1 mol L^{-1} TBAP/CH_3CN.

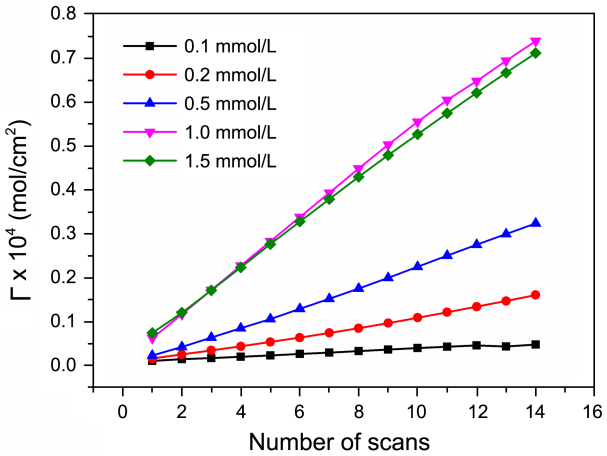

Figure 2. Graph of the apparent surface coverage *vs.* the scan number for the oxidative polymerization of Ni(saldMp) in 0.1 mol L^{-1} TBAP/CH_3CN. The concentrations of Ni(saldMp) are 0.1 mmol L^{-1}, 0.2 mmol L^{-1}, 0.5 mmol L^{-1}, 1.0 mmol L^{-1} and 1.5 mmol L^{-1}. The scan rate is 20 mV s^{-1}.

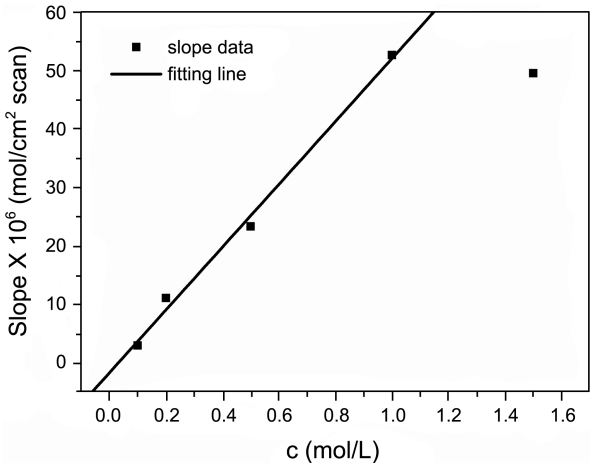

Figure 3. Graph of the slope (obtained from the data in Figure 2) *vs*. concentration for the oxidative polymerization of Ni(saldMp).

However, the poly[Ni(saldMp)] growth rate does not increase obviously when the concentration increases to 1.5 mmol L^{-1}, which is partly attributed to the increased difficulty in diffusion Ni(saldMp) monomer resulting from the high concentration of Ni(saldMp). Moreover, a high Ni(saldMp) concentration provides more monomer to participate the polymerization reaction, as well as induces the competition of reaction for monomers.

Figure 4 shows the morphologies of the poly[Ni(saldMp)] samples with different monomer concentrations. Basically, it can be seen the tube structure of MWCNTs in the electrode samples. From Figure 4, it is obvious that poly[Ni(saldMp)] grows with the MWCNTs as a skeleton, and the increase of the diameter and links on MWCNTs as well as the decrease of gaps on the surface of the electrode reflect the increase

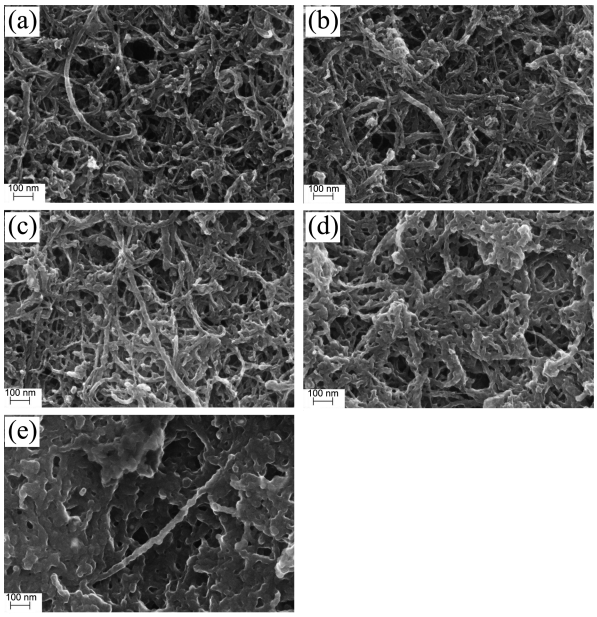

Figure 4. FESEM images of the poly[Ni(saldMp)] samples deposited with different monomer concentrations. (a) 0.1 mmol L^{-1}, (b) 0.2 mmol L^{-1}, (c),0.5 mmol L^{-1}, (d) 1.0 mmol L^{-1} and (e) 1.5 mmol L^{-1}.

of the mass of the as-grown poly[Ni(saldMp)] with the Ni(saldMp) concentration increasing. The result is in conformity with that of the apparent surface coverage. In Figure 4(e), the poly[Ni(saldMp)] almost fill all the electrode surface gaps and form a relatively dense structure, which seems to reveal much more poly[Ni(saldMp)] on MWCNTs than that in Figure 4(d). Combined the data in Figure 2, there seems to be a contradictory. The apparent surface coverages are similar between the Ni(saldMp) concentrations 1.0 mmol L^{-1} and 1.5 mmol L^{-1}, which indicates an approximate value of the poly[Ni(saldMp)] mass deposited on MWCNTs. It could be interpreted by the cross-linkage between pendant saldMp moieties during the irreversible structure reorganization processes, which is susceptible to occur with a higher monomer concentration. This is in agreement with the increase in the current of the extra oxidation peak in Figure 1. Once the cross-linkage fill all the gaps on the MWCNTs to form an entire polymer film, the electronic diffusion will be hindered, and in return the electrochemical activity of poly[Ni(saldMp)] will be reduced. Considering all the above-mentioned factors, it could be drawn that the suitable concentration for electrodeposition of Ni(saldMp) on MWCNTs is 1.0 mmol L^{-1}.

Effect of Potential Windows on Charge-Discharge Efficiencies. The typical cyclic voltammograms of MWCNTs and poly[Ni(saldMp)] coated MWCNTs electrodes (pMWCNTs) under different potential ranges at the scan rate of 80 mV s^{-1} are shown in Figure 5. From the CV plots of pMWCNTs and MWCNTs, it should be noted that portion of 0.0-0.4 V has no obvious change whereas the area of responsive currents of pMWCNTs electrodes during all the scan ranges completely cover that of the MWCNTs electrode, which indicates that the polymerization of Ni(saldMp) on MWCNTs slightly positives the double-layer absorption and desorption process on the surface of MWCNTs substrate. Besides, the portion from 0.4 V to 1.2V of pMWCNTs electrode may be viewed as the sum of the double-layer absorption/desorption current of MWCNTs substrate and the faradic current of

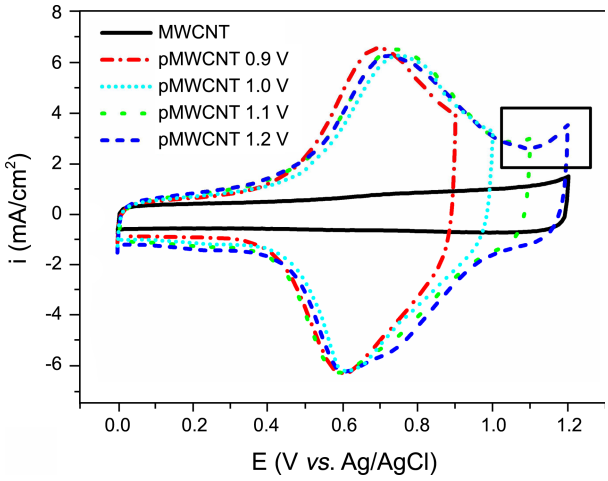

Figure 5. Cyclic voltammograms of MWCNTs and poly[Ni(saldMp)]/MWCNTs electrodes under different potential ranges in 1 mol L^{-1} Et_3MeNBF_4/AN solution. Scan rate: 80 mV s^{-1}.

poly[Ni(saldMp)]. The redox couple observed in Figure 5 is assigned to the Ni(II)/Ni(III) redox process of the nickel centre of poly[Ni(saldMp)]. The larger areas of responsive currents reveal that the pMWCNTs electrode has larger charge storage ability than the pure MWCNTs electrode.

The pMWCNTs electrodes possess a couple of redox peaks at 0.7 V and 0.6 V in Figure 5, which associates with the oxidation/reduction state transition process in poly[Ni-(saldMp)] lm. All the current responses of poly[Ni(saldMp)] electrodes exhibit similar peak currents, whereas the curve of electrode under 0.0-0.9 V shows the best reversibility. When the sweep ranges of CV for the pMWCNTs electrode are subsequently enlarged from 0.0-0.9 V to 0.0-1.2 V, the shape of reduction waves becomes wide slightly, but the oxidation current begins to increase as the potential increases higher than 1.0 V, which may indicts the over oxidation of poly[Ni(saldMp)].

Figure 6 shows the galvanostatic charge/discharge curves of the pMWCNTs electrode at the current density of 0.05 mA cm^{-2} under different potential ranges. Compared with the curves of MWCNTs electrode, the charge and discharge time of pMWCNT electrodes are much longer, and it demonstrates clearly that the total capacitance increases with the loading of poly[Ni(saldMp)]. When the potential range enlarges from 0.0-0.9 V to 0.0-1.2 V, discharging time varies within 150 s, whereas the charging time increases greatly from about 600 s to over 1500 s. This shows a decrease in the charging/discharging efficiency of the pMWCNTs electrode with the enlargement of potential window.

Hence, the dependence of the charge-discharge efficiency on the current density is plotted in Figure 7 with different potential windows. The charge-discharge efficiencies increase with the increased current density and then keep on a steady value with all the potential windows except that between 0.0-0.9 V. The charge-discharge efficiency reaches a maximum value at the current density of 1.00 mA cm^{-2} and then decreases with the increase of the current density, which may indicate that under this potential window the redox

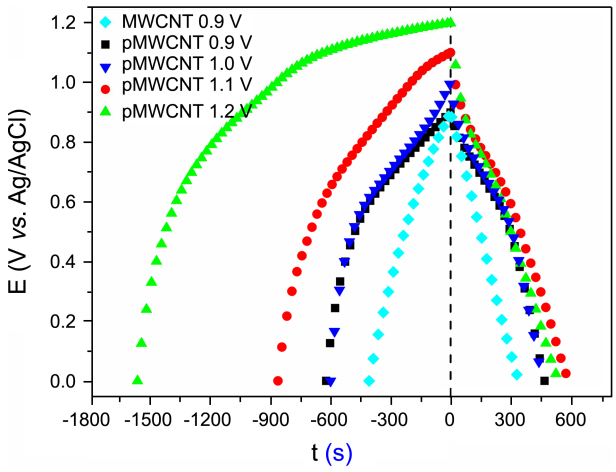

Figure 6. Galvanostatic charge/discharge curves of the pMWCNTs electrode at the current density of 0.05 mA cm^{-2} under different potential ranges.

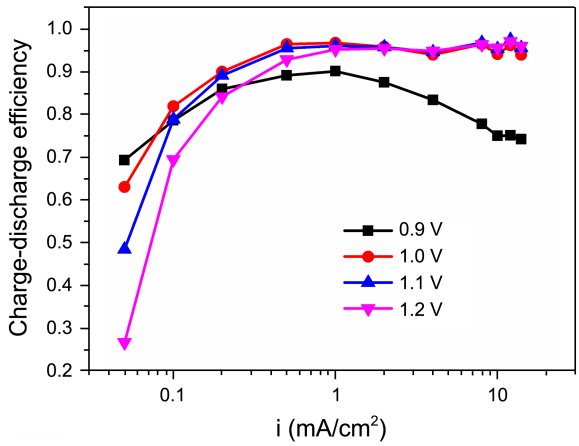

Figure 7. Charge-discharge efficiency *vs.* current density with different potential windows.

capacitance of poly[Ni(saldMp)] is not fully realized. By comparison of the curves with the potential window 0.0-1.0 V, 0.0-1.1 V and 0.0-1.2 V, it can be seen that the charge/discharge efficiency is the highest under the potential range from 0.0 to 1.0 V, which manifests the best charge storage and release ability of pMWCNTs electrode at 0.0-1.0 V.

Effect of Electrodeposition Scan Number on Capacitance Performance. In order to evaluate the mass of poly-[Ni(saldMp)] influence on capacitance performance, the effect of electrodeposition scan number is analysed at the potential window 0.0-1.0 V, and the electrodeposition concentration of Ni(saldMp) is 1.0 mmol L^{-1}. Samples with different electrodeposition scan number of 2, 4, 6, 8, 10, 12 and 14 are labeled as S2, S4, S6, S8, S10, S12 and S14, respectively.

The doping level can be used for investigating quantitatively the electrochemical activity of conducting polymer, which means the relative charge stored per monomer unit inside conducting polymer.[33-37] The mass of as-grown poly-[Ni(salen)] is evaluated by the calculation of charge depleted during the electropolymerization. Figure 8 shows the evolutions of the doping level and mass of poly[Ni(salen)] grown on MWCNTs electrode. It is obvious that the mass of poly-

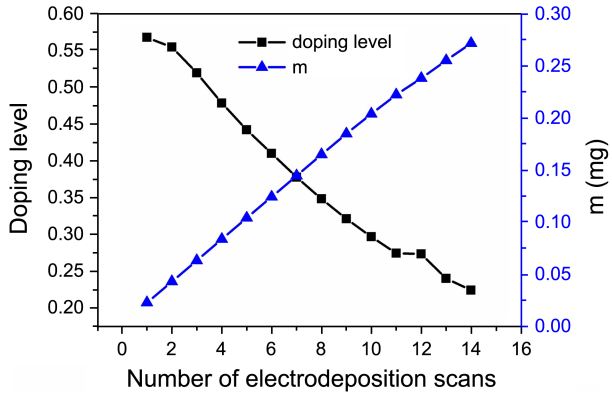

Figure 8. Doping level and mass of poly[Ni(saldMp)] grown on MWCNTs electrode *vs.* electrodeposition scan number with the monomer concentration of 1 mmol L^{-1}.

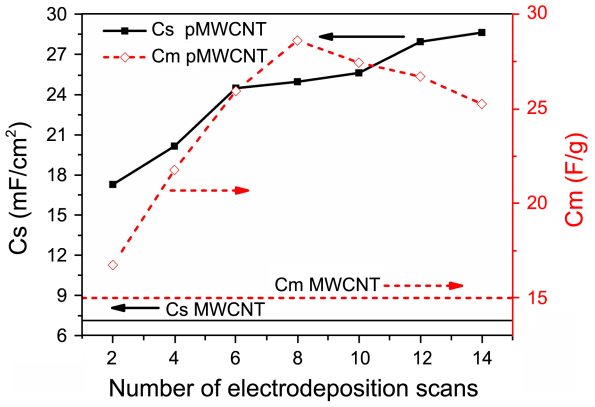

Figure 9. Geometric specific capacitance and gravimetric specific capacitance of pMWCNTs electrodes with different deposition scan numbers at the current density of 0.10 mA cm^{-2}.

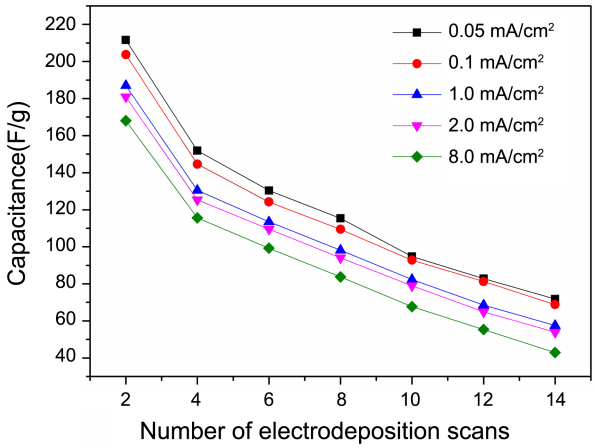

Figure 10. Capacitance-deposition scan number relationship of poly[Ni(saldMp)] at different current densities calculated from charge/discharge tests after subtracting the capacitance of MWCNTs from the total capacitance.

[Ni(saldMp)] increases with the number of deposition scans increasing, which reflects that the influence of monomer diffusion is non- control factor with the concentration of 1.0 mmol L^{-1}. Nevertheless, the doping level of poly[Ni-(saldMp)] decreases with the increased number of electro-deposition scans, and it indicates that the poly[Ni(saldMp)] prepared with less deposition scans possesses higher charge storage ability. It would be partly interpreted by the impeding charge diffusion with the continuously depositing of Ni(saldMp) onto the MWCNTs surface. Moreover, when the electrodeposition scan number increases, the former deposited poly[Ni(saldMp)] will be partially blocked by the latter ones, which also induces to the decrease in the doping level.

Figure 9 shows the gravimetric and geometric specific capacitances of pMWCNTs electrodes with different deposition scan numbers at the current density of 0.10 mA cm^{-2}, and the corresponding values of MWCNTs are given to illustrate the increase of the gravimetric and geometric specific capacitances. It is evident that the geometric specific capacitance increases because of the loading of poly[Ni-(saldMp)], as well as the gravimetric specific capacitance, which indicates the redox capacitance contribution of poly[Ni(saldMp)] on total capacitance of the electrode as described in Figure 5. However, the gravimetric specific capacitance increases to a maximum value of 28.6 F g^{-1} (1.24 times as that of the bare MWCNTs electrode) with sample S8 and then decreases as the number of deposition scans increases. And the geometric specific capacitance of S8 is 25.0 mF cm^{-2}, 3.53 times as high as that of the bare MWCNTs electrode. Since the capacitance increase results from the as-prepared poly[Ni(saldMp)] on the bare MWCNTs electrode, it is inevitable that the decrease in capacitance of electrode with increasing deposition scan numbers is caused by the poly[Ni(saldMp)] itself.

The capacitances of poly[Ni(saldMp)] at different charge/discharge current densities calculated from charge/discharge tests after subtracting the capacitance of MWCNTs from the total capacitance are showed in Figure 10. The specic capacitance of poly[Ni(saldMp)] is 212, 152, 130, 115, 95, 83 and 72 F g^{-1} at the current density of 0.05 mA cm^{-2} for S2, S4, S6, S8, S10, S12 and S14, respectively. The specic capacitance of poly[Ni(saldMp)] at all different current densities decreases with the increasing number of electro-deposition scans, indicating the decrease of electrochemical activity in accordance with the doping level of poly[Ni-(saldMp)] stated in Figure 8. It can be seen that sample S2 exhibits higher specic capacitance than other samples at all discharge current densities, and the specic capacitance of S2 is 212, 204, 187, 180, and 168 F g^{-1} at the current densities of 0.05, 0.10, 1.00, 2.00 and 8.00 mA cm^{-2}, respectively, as shown in Figure 10. For a single sample, the specific capacitance decreases with the charge/discharge current density increases, and the plot of retention rate *vs.* current density is used to evaluate the capacitance performance of poly[Ni(saldMp)] at different current densities (Figure 11).

The capacitance retention rate was calculated from the ratio of capacitance values at a higher current density and 0.05 mA cm^{-2}. It is clear that the retention rate decreases

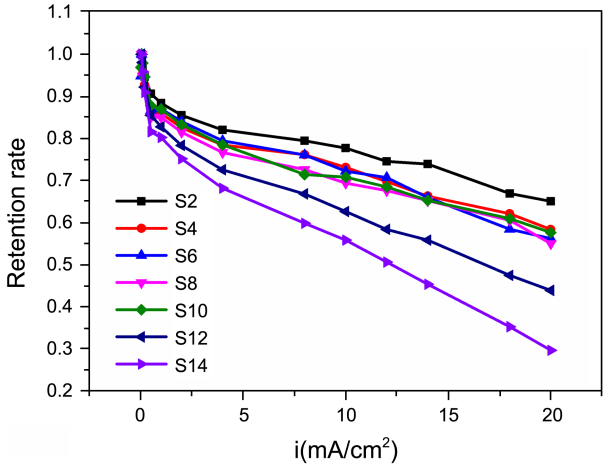

Figure 11. The capacitance retention rate of poly[Ni(saldMp)] with the different charge/discharge current densities. The capacitance value at 0.05 mA cm^{-2} was set as a reference point.

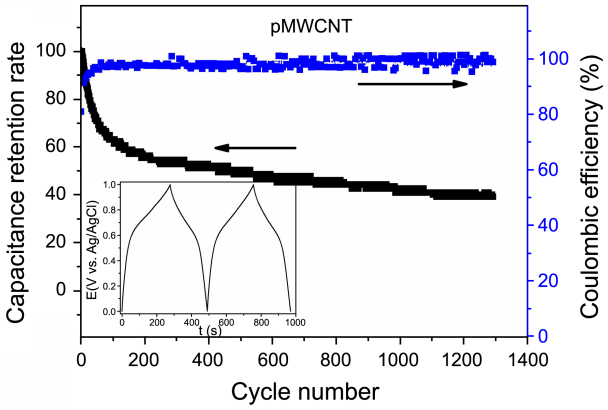

Figure 12. Variation of the discharge capacitance retention rate and coulombic efficiency with the number of constant current cycles at about 0.1 mA cm^{-2}.

with the increasing current density, which is in conformity with the capacitance decrease in Figure 10. Poly[Ni-(saldMp)] prepared with more deposition scan numbers possesses lower retention rate at a particular current density, which could be expressed by the diffusion difficulty in the electrode with more poly[Ni(saldMp)] coated at high current densities. It is worth noting that poly[Ni(saldMp)] prepared with 4, 6, 8 and 10 electrodeposition scan numbers exhibit similar retention rate variation with the increasing current densities, which indicates similar diffusion ability with this four electrodes. Thus, 8 is the reasonable number of electrodeposition scans for preparing poly[Ni(saldMp)] on MWCNTs.

The cycle characterization of the poly[Ni(saldMp)] coated electrode, which was prepared at 0.1 mA cm^{-2}, is presented in Figure 12. The specific capacitance decreased rapidly in prior 100 cycles (63.2% retained), and then it kept acceptable stability from 100 cycles to 1300 cycles. After 1300 cycles, the poly[Ni(saldMp)] modified electrode retained about 39.3% of initial specific capacitance and the coulomb efficiency was broadly stable. This implied that the charge-discharge cycle stability of the poly[Ni(saldMp)] coated MWCNT electrode was not perfect.Part of the reason may be related to the matching of supporting electrolyte and the polym[Ni(saldMp)]. How to improve the cycle stability will be the next subject of further studies.

Conclusions

Poly[Ni(saldMp)] was deposited on MWCNTs substrate *via* dynamic potential scanning. The optimum condition of Ni(saldMp) electrodeposition on MWCNTs is with monomer concentration of 1.0 mmol L^{-1} by 8 deposition scans and tested between 0.0-1.0 V, under which the geometric specific capacitance of poly[Ni(saldMp)] coated electrode is 3.53 times as high as that of pure MWCNTs, and 1.24 times for gravimetric specific capacitance. And the poly[Ni(saldMp)] itself exhibits a good capacitance performance with a highest value of 212 F g^{-1} at the current density of 0.05 mA cm^{-2}. The capacitance performances of poly[Ni(saldMp)] at different current densities make it a promising conducting polymer for supercapacitors, and the electrochemical capacitance increase by incorporating poly[Ni(saldMp)] of reasonable mass on MWCNTs demonstrates the possibility of open the way to enhance the charge storage ability for supercapacitors.

Acknowledgments. Financial supports of this work by Program for New Century Excellent Talents in University (NECT) and State Key Laboratory of Multiphase Complex Systems (MPCS-2011-D-08) are gratefully acknowledged.

References

1. Justin, P.; Ranga Rao, G. *Int. J. Hydrogen. Energy* **2010**, *35*, 9709.
2. Hou, Y.; Cheng, Y.; Hobson, T.; Liu, J. *Nano Lett.* **2010**, *10*, 2727.
3. Yu, P.; Zhang, X.; Chen, Y.; Ma, Y. *Mater. Lett.* **2010**, *64*, 1480.
4. Yang, M. Y.; Ni, P.; Li, Y.; He, X. X.; Liu, Z. H. *Mater. Chem. Phys.* **2010**, *124*, 155.
5. Yan, J.; Wei, T.; Cheng, J.; Fan, Z. J.; Zhang, M. L. *Mater. Res. Bull.* **2010**, *45*, 210.
6. Xu, M. W.; Jia, W.; Bao, S. J.; Su, Z.; Dong, B. *Electrochim. Acta* **2010**, *55*, 5117.
7. Yan, X.; Tai, Z.; Chen, J.; Xue, Q. *Nanoscale* **2011**, *3*, 212.
8. Yuan, J. K.; Dang, Z. M.; Yao, S. H.; Zha, J. W.; Zhou, T.; Li, S. T.; Bai, J. B. *J. Mater. Chem.* **2010**, *20*, 2441.
9. Wang, H.; Hao, Q.; Yang, X.; Lu, L.; Wang, X. *ACS Appl. Mater. Interfaces* **2010**, *2*, 821.
10. Wang, H.; Hao, Q.; Yang, X.; Lu, L.; Wang, X. *Nanoscale* **2010**, *2*, 2164.
11. Liu, R.; Duay, J.; Lee, S. B. *ACS Nano* **2010**, *4*, 4299.
12. Wang, M. X.; Wang, C. Y.; Chen, M. M.; Wang, Y. S.; Du, X.; Li, T. Q.; Hu, Z. J. *New Carbon Mater.* **2010**, *25*, 285.
13. Byon, H. R.; Lee, S. W.; Chen, S.; Hammond, P. T.; Shao-Horn, Y. *Carbon* **2011**, *49*, 457.
14. Fu, Q.; Gao, B.; Dou, H.; Hao, L.; Lu, X.; Sun, K.; Jiang, J.; Zhang, X. *Synthetic. Met.* **2011**, *161*, 373.
15. Geng, X.; Li, F.; Wang, D.-W.; Cheng, H.-M. *Carbon* **2012**, *50*, 344.
16. Chen, Y.; Zhang, X.; Yu, P.; Ma, Y. *J. Power Sources* **2010**, *195*, 3031.
17. Du, X.; Guo, P.; Song, H.; Chen, X. *Electrochim. Acta* **2010**, *55*, 4812.
18. Liu, J.; Sun, J.; Gao, L. *J. Phys. Chem. C* **2010**, *114*, 19614.
19. Lee, S. W.; Kim, J.; Chen, S.; Hammond, P. T.; Yang, S. H. *ACS Nano* **2010**, *4*, 3889.
20. Peng, C.; Hu, D.; Chen, G. Z. *Chem. Commun.* **2011**, *47*, 4105.
21. Lang, X.; Zhang, L.; Fujita, T.; Ding, Y.; Chen, M. *J. Power Sources* **2012**, *197*, 325.
22. Zou, B.; Liang, Y.; Liu, X.; Diamond, D.; Lau, K. *J. Power Sources* **2011**, *196*, 4842.
23. Liu, W.; Liu, N.; Song, H.; Chen, X. *New Carbon Mater.* **2011**, *26*, 217.
24. Wang, Y.; Yang, C.; Liu, P. *Chem. Eng. J.* **2011**, *172*, 1137.
25. Jin, M.; Han, G.; Chang, Y.; Zhao, H.; Zhang, H. *Electrochim. Acta* **2011**, *56*, 9838.
26. Hou, L.; Yuan, C.; Li, D.; Yang, L.; Shen, L.; Zhang, F.; Zhang, X. *Electrochim. Acta* **2011**, *56*, 6049.
27. Shang, K.; Ai, S.; Ma, Q.; Tang, T.; Yin, H.; Han, H. *Desalination* **2011**, *278*, 173.
28. Lowe, M. A.; Kiya, Y.; Henderson, J. C.; Abruña, H. D. *Electrochem. Commun.* **2011**, *13*, 462.
29. Hoferkamp, L. A.; Goldsby, K. A. *Chem. Mater.* **1989**, *1*, 348.
30. Tchepournaya, I.; Vasilieva, S.; Logvinov, S.; Timonov, A.; Amadelli, R.; Bartak, D. *Langmuir* **2003**, *19*, 9005.

31. Gao, F.; Li, J.; Zhang, Y.; Wang, X.; Kang, F. *Electrochim. Acta* **2010**, *55*, 6101.
32. Petr, A.; Dunsch, L.; Neudeck, A. *J. Electroanal. Chem.* **1996**, *412*, 153.
33. Aubert, P. H.; Audebert, P.; Roche, M.; Capdevielle, P.; Maumy, M.; Ricart, G. *Chem. Mater.* **2001**, *13*, 2223.
34. Vilas-Boas, M.; Freire, C.; de Castro, B.; Hillman, A. R. *J. Phys. Chem. B* **1998**, *102*, 8533.
35. Tedim, J.; Carneiro, A.; Bessada, R.; Patrício, S.; Magalhães, A. L.; Freire, C.; Gurman, S. J.; Hillman, A. R. *J. Electroanal. Chem.* **2007**, *610*, 46.
36. Martins, M.; Boas, M. V.; de Castro, B.; Hillman, A. R.; Freire, C. *Electrochim. Acta* **2005**, *51*, 304.
37. Vilas-Boas, M.; Santos, I. C.; Henderson, M. J.; Freire, C.; Hillman, A. R.; Vieil, E. *Langmuir* **2003**, *19*, 7460.